energies

MDPI

Article

Xerogel-like Materials from Sustainable Sources: Properties and Electrochemical Performances

Gisele Amaral-Labat [1], Manuella Gobbo C. Munhoz [2], Beatriz Carvalho da Silva Fonseca [1], Alan Fernando Ney Boss [2], Patricia de Almeida-Mattos [2], Flavia Lega Braghiroli [3,*], Hassine Bouafif [3], Ahmed Koubaa [4], Guilherme F. B. Lenz e Silva [2] and Maurício Ribeiro Baldan [1]

1 Instituto Nacional de Pesquisas Espaciais, Av. dos Astronautas, 1758, Jardim da Granja, São José dos Campos 12227-010, SP, Brazil; gisele.amarallabat@gmail.com (G.A.-L.); beatriz.csilvafonseca@gmail.com (B.C.d.S.F.); mrbaldan2@yahoo.com (M.R.B.)
2 Departamento de Engenharia Metalúrgica e de Materiais (PMT), Universidade de São Paulo (USP), Avenida Mello Moraes, 2463, Cidade Universitária, São Paulo 05508-030, SP, Brazil; manuellagobbo@usp.br (M.G.C.M.); alan.boss@usp.br (A.F.N.B.); s.patricialmeida@gmail.com (P.d.A.-M.); guilhermelenz@usp.br (G.F.B.L.e.S.)
3 Centre Technologique des Résidus Industriels, Cégep de l'Abitibi-Témiscamingue, 425 Boul. du Collège, Rouyn-Noranda, QC J9X 5E5, Canada; hassine.bouafif@cegepat.qc.ca
4 Institut de recherche sur les forêts, Université du Québec en Abitibi-Témiscamingue, 445 Boul. University, Rouyn-Noranda, QC J9X 5E4, Canada; ahmed.koubaa@uqat.ca
* Correspondence: flavia.braghiroli@cegepat.qc.ca; Tel.: +1-(819)-762-0931 (ext. 1748)

Abstract: Energy storage is currently one of the most significant technological challenges globally, and supercapacitor is a prominent candidate over batteries due to its ability for fast charging and long lifetime. Supercapacitors typically use porous carbon as electrodes, because of both the high conductivity and surface area of the material. However, the state-of-the-art porous carbon described in the literature uses toxic chemicals and complex procedures that enhance costs and pollute the environment. Thus, a more sustainable procedure to produce porous carbon is highly desirable. In this context, xerogel-like carbons were prepared by a new, cheap, simple route to polymerization reactions of tannin-formaldehyde in a bio-oil by-product. Using bio-oil in its natural pH allowed a cost reduction and avoided using new reactants to change the reactional medium. Textural properties and electrochemical performances were improved by fast activating the material per 20 min. The non-activated carbon xerogel presented a capacitance of 92 F/g, while the activated one had 132 F/g, given that 77% of the components used are eco-friendly. These results demonstrate that renewable materials may find applications as carbon electrodes for supercapacitors. Overhauling the synthesis route with a different pH or replacing formaldehyde may enhance performance or provide a 100% sustainable carbon electrode.

Keywords: xerogel-like materials; tannin; bio-oil; biosourced porous carbon; electrochemical performances

Citation: Amaral-Labat, G.; Munhoz, M.G.C.; Fonseca, B.C.d.S.; Boss, A.F.N.; de Almeida-Mattos, P.; Braghiroli, F.L.; Bouafif, H.; Koubaa, A.; Lenz e Silva, G.F.B.; Baldan, M.R. Xerogel-like Materials from Sustainable Sources: Properties and Electrochemical Performances. *Energies* **2021**, *14*, 7977. https://doi.org/10.3390/en14237977

Academic Editor: Wei-Hsin Chen

Received: 29 September 2021
Accepted: 20 November 2021
Published: 29 November 2021

1. Introduction

Clean energy generation is one of the hot topics in academic research, and both wind and solar energy systems are intermittent and seasonal. An alternative solution is to store energy to use during periods in which it cannot be generated. Li-ion or lead-acid batteries could store energy, but they are heavy, slow-chargers, have a low lifetime, and contain toxic elements. Supercapacitors have the capacity to overcome the issues involved with batteries because they can charge faster, are lighter, have a greater lifetime, and can be made of porous carbon [1]. Today, supercapacitors can cost 20 times more than a Li-ion battery and 100 times more than a lead-acid battery. One reason is that the porous carbon materials used in supercapacitors are expensive to produce, may cause equipment corrosions, and produce toxic by-products that require appropriate disposal [2]. Complex production strategies to

make high surface area porous carbon, such as metal-organic frameworks, contribute to the high costs [3,4]. Moreover, clean energy storage devices should not generate pollution by using waste, recycled materials or by-products during production.

A great alternative that can be used to create porous carbon materials, commonly known as biochars [5], is the thermochemical conversion of biomass, a rich-carbon renewable organic matter. Biochars have several applications that are described in the literature, such as CO_2 capture through adsorption [6], soil amendment [7], or heavy metal removal from wastewater [8]. Other by-products could be generated during biomass's thermochemical conversion, such as syngas, synthesis gas, and bio-oil. The latter may contain different types of compounds, like lignin-derived oligomers, acids, alcohols, phenols, aldehydes, and others, depending on the biomass feedstock and pyro-gasification conditions. To date, bio-oil can be used as liquid smoke and wood flavor, adhesives for asphalt bio-binder, biodegradable polymers, resins, combustive for furnace, polyurethane and biocarbon electrodes [9–11].

The most desirable feature for a carbon electrode is the high surface area, which is achieved with a good distribution of micro and mesopores. Different compounds present in biomass and bio-oil offer challenges to developing suitable porous carbon for energy storage. The synthesis route is crucial to determine porosity, produced by one or more mechanism, such as carbonization-activation, template-assisted carbonization, new activation agents, self-template, direct pyrolysis of copolymer, self-activation, and laser scribing [2].

There are few pieces of research in the literature about the electrochemical performance of porous carbon made from bio-oil. Most use one or more techniques to enhance performance, such as chemical activation, doping, or template [12–17]. However, several steps that are used to produce suitable properties increase the final cost of the porous carbon and represent a limiting factor in terms of scaling-up production.

Several efforts have been dedicated to using sustainable sources, such as biomasses, wastes, and by-products, to develop cheaper, renewable porous carbon materials for energy storage devices. One of these efforts is to reduce the usage of expensive, synthetic, toxic compounds, such as phenol and resorcinol. Tannin is a natural biopolymer polyphenolic-based compound that could replace the aforementioned compounds [18]. It is well established that tannin-formaldehyde reactions produce porous carbon materials, especially gels [19] and foams [20]. Generally, the production of tannin-gels uses pure water [21], mixtures of water:ethanol [22,23] or water:methanol [24,25] as solvents, and the reactions may occur in large ranges of mass ratio (4–40%) and pH (2–10), controlled by the addition of alkali and acid [24]. Furthermore, most tannin-gels are dry under supercritical CO_2 drying, where it is mandatory to use pressure, temperature, and solvent exchange, increasing preparation steps and costs.

This work describes a simple synthesis route to make a gel-like material based on tannin-formaldehyde reactions using bio-oil from *Tilia Americana* softwood residue as a carbon-rich solvent and PMMA (Poly(methyl methacrylate)) as a shrinkage prevention agent. The main aspects approached were: (i) producing xerogel-like sustainable porous carbon through subcritical drying through a fast and simple methodology; (ii) combining cheap, renewable, non-toxic, and natural phenolic with bio-oil, a by-product of fast-pyrolysis of *Tilia Americana* wood residue; and (iii) evaluating the performance of CO_2-activated material and its carbonized precursor as electrodes for supercapacitors.

2. Materials and Methods

2.1. Raw Materials

The condensed tannin powder from *Acacia mearnsii*, commercially identified as WEIBULL AQ and the microspheres of PMMA (Poly(methyl methacrylate)) were kindly provided by TANAC S.A. (Montenegro, RS, Brazil) and UNIGEL Ltda. (São Paulo, SP, Brazil), respectively. The tannin powder was industrially extracted from tree barks from planted forests

dedicated to manufacturing tannins, chips, and wood pellets. The PMMA microspheres were manually classified by sieving, presenting diameters ranging from 800 to 100 µm.

The bio-oil used in this study was supplied by ABRI-Tech Inc. (Namur, QC, Canada). The primary biomass feedstock, *Tilia Americana* wood residue, was converted into bio-oil using an industrial scale auger fast pyrolysis reactor at temperatures ranging from 400 to 500 °C.

2.2. Bio-Oil Characterization

The density and lignin content of the crude bio-oil measured by pycnometer bottles and gravimetric methodology, respectively, are described elsewhere [9]. Briefly, the volume and weight of five samples of bio-oil were accurately measured to calculate the density. The lignin content was investigated by adding bio-oil in water (3:1) under rigorously magnetic stirring at an ambient temperature and was then left to decant for two hours, forming two phases: the top, aqueous phase containing water-soluble compounds; and the bottom, solid, carbon-rich, called pyrolytic lignin. After removing the soluble products, the solid phase was dried in an oven for 24 h at 40 °C.

2.3. Xerogel-like Synthesis

Gel-like materials were prepared by dissolving 6 g of tannin in 30 g of raw bio-oil and introducing 12 g (37 wt.%) of an aqueous solution of formaldehyde and 12 g of PMMA into the solution. The reaction was performed under continuous stirring at 85 °C until the mixture's gelation was completed after five hours. After gelation, the material was naturally air-dried for five days and then left in an oven for 24 h at 103 °C to ensure total drying. A different formulation was made without PMMA to estimate the preserved porosity avoided by these polymeric spheres. Volumetric measurements were employed to control the shrinkage of the xerogel-like material before and after drying. The final hard, black solid was placed in alumina crucibles, heated at 10 °C/min up to 900 °C in a tubular oven, and kept for two hours. The carbonized xerogel-like material was hand-grinded, classified through a 100 µm sieve and labeled XGL-C. Particles smaller than 100 µm were activated under a CO_2 atmosphere at 1000 °C for 20 min, and the final powder was labeled XGL-AC. The synthesized materials and their following physicochemical analyses were repeated three times.

2.4. Chemical, Morphological and Textural Analysis

A high-resolution field emission gun scanning electron microscopy (FEG-SEM) (TESCAN microscope, model MIRA3) and a Transmission Electron Microscopy (TEM) FEI Tecnai Spirit BioTwin (120 kV) were used for morphological analysis.

A Fourier transform infrared spectrometer (FTIR) (Agilent, Cary 660) was used for spectral acquisition, recorded with a spectral resolution of 4 cm^{-1} between 4000 and 400 cm^{-1} by averaging 20 scans. The FTIR analysis samples consist of pellets with 2 mg of XGL, tannin, or bio-oil mixed with 200 mg of potassium bromide (KBr) in a spectroscopy grade. Each sample was mixed, ground, and pressed for producing the pellets. KBr, tannin, bio-oil, and XGL were dried at 100 °C for 24 h previously.

The nitrogen adsorption/desorption isotherms were recorded in a Micromeritics ASAP 2020 Plus instrument at −196 °C. First, the samples XGL-C e XGL-AC were outgassed for 24 h at 200 °C. The specific surface area (S_{BET}) and micropores volume (V_{DR}) were calculated through Brunauer-Emmet-Teller [26] and Dubinin-Radushkevic [27] methods, respectively. The estimated mesopore volume was calculated by the difference between the total pore volume adsorbed at P/P_0 = 0.97 and the micropores volume ($V_{meso} = V_{0.97} - V_{DR}$). The density functional theory (DFT) was applied to calculate the pore-size distribution (PSD).

Differential thermal analysis (DTG) was performed in a TA Instruments SDT-650, using a temperature range from 40 to 1100 °C and a heating rate of 5 °C/min under a nitrogen atmosphere.

Elemental analysis (CNH) was used to determine carbon, nitrogen, and hydrogen concentrations in the xerogel-like carbons, using 10 mg of sample in an elemental analyzer (Perkin Elmer 2400 series ii). The carbon samples were placed in a tin capsule and sintered at 925 °C under an oxygen atmosphere. The oxygen content was calculated by the difference (%O = 100 − %CHN).

2.5. Electrochemical Characterization

The electrochemical characterization was performed with an Autolab PGSTAT 302N. A conventional three-electrode electrochemical cell was prepared using a platinum plate as a counter electrode and Ag/AgCl saturated KCl as a reference electrode in an aqueous electrolyte KOH 6 mol/L. The Ag/AgCl saturated KCl electrode was always calibrated with a saturated calomel electrode, before and after all of the electrochemical characterizations [28,29]. The carbon electrodes were prepared by an ultrasonic suspension containing 15 mg of XGL-C or XGL-AC materials, Nafion 5 wt.% (50 µL), and ethylene glycol (100 µL). The suspension was deposited on a graphite plate and dried at 90 °C for two hours. Cyclic voltammetry (CV) tests were performed at scan rates between 1 and 200 mV/s within the potential range of -1 to 0 V. The voltage range used to test the cells corresponds to the maximum potential window used for aqueous electrolytes. Galvanostatic charge-discharge (GCD) experiments were carried out at constant density currents ranging from 0.05 to 20 A/g, based on the total mass of the electrode. The cycling stability was studied through GCD tests up to 1000 charge-discharge cycles at 1 A/g current density.

The specific capacitance (Cs, F/g) was calculated from the galvanostatic discharge curves using Equation (1):

$$Cs = \frac{I.\,\Delta t}{m.\,\Delta V} \quad (1)$$

where I is the discharge current, t is the discharge time, V is the voltage change, and m is the electrode active material mass.

The energy and power densities were determined from capacitance and the electrochemical voltage window. The energy (E, Wh/kg) and power (P, W/kg) densities were calculated using Equations (2) and (3), respectively:

$$E = \frac{1}{2 \times 3.6} C_S.(\Delta V)^2 \quad (2)$$

$$P = 3600\, x \frac{E}{\Delta t_D} \quad (3)$$

The electrochemical impedance spectroscopy (EIS) measurements were performed at an open-circuit voltage (OCP) in the frequency range of 100 kHz to 1 mHz with an alternation current amplitude of 5 mV. The EIS data were analyzed by using Nyquist plots.

3. Results and Discussion

3.1. Bio-Oil Properties and Condensation Reactions

Bio-oil is a carbon-rich by-product, mainly due to its significant lignin content, presenting a high content of reactive oxygen groups, from 23 to 35 wt.% according to the biomass source [30]. Those oxygen groups are suitable for polymerization reactions with formaldehyde, especially because the -OH groups from phenolic compounds, such as resorcinol and phenol, induce reactions in *ortho*- and *para*- positions in phenolic rings by methylene bridges [31,32]. Furthermore, C=O groups from carbonyl and unconjugated ketones might also participate in forming the crosslinks to create the network [33]. The mixture of water with bio-oil allows the precipitation of a reactive hydrophobic organic matter, mainly composed of lignin molecules. Thus, the reactive matter of the bio-oil used in this study was about 31 wt.% ± 3.

The calculated density of the liquid by-product at 20 °C was 1.11 g/cm^3, which agrees with values found for bio-oil from softwood (1.16 g/cm^3). The bio-oil presented a pH of 2.3 and, thus, was within the range considered corrosive (2 to 3.7) [34]. Hence,

disposal or management of such liquid represents additional handling costs. However, tannin-formaldehyde reactions can work in an extensive pH range, including at a corrosive level [24]. Therefore, all of the reactions were performed at the actual pH of the bio-oil. Figure 1 presents the curves of FTIR and TG/DTG analyses of bio-oil, tannin and XGL. While FTIR presents the main chemical differences, TG/DTG analysis shows the primary thermal decomposition of the raw materials and the final XGL product. By comparing the curves of the three materials, the polymerization reactions could be evaluated during the gel synthesis. Thus, the lignocellulosic matter, naturally found in bio-oil, could also participate in the polymerization process by reactions of tannin-formaldehyde-organic compounds, especially the phenolic groups, as already observed for synthetic [21,35], natural [18] and raw compounds, like black liquor [36].

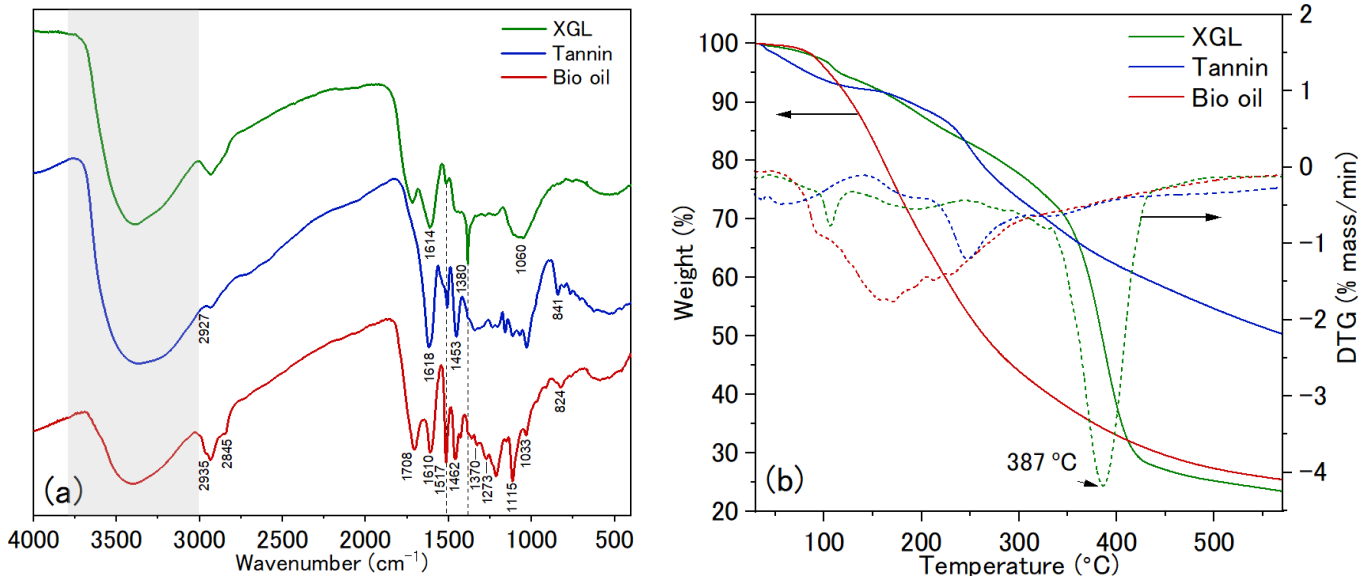

Figure 1. (**a**) FTIR spectra and (**b**) thermal analysis TG/DTG of bio-oil, tannin and XGL.

Table 1 lists the prominent peaks found for bio-oil [9] and tannin [37]. The new, distinct peak at 1380 cm^{-1} appears on the spectrum of XGL and could be assigned to CH_2 and CH_3 in the methylene bridges from phenolic resins [38], while a large band is found on the region of the C-O stretching centered at 1060 cm^{-1} [39]. Furthermore, the peak at 1517 cm^{-1} which is attributed to lignin derivatives [40] presented on the bio-oil spectrum also decreases on the XGL curve. The aromatic C-H stretching at 841 cm^{-1}, observed in the tannin spectrum, is not seen in XGL. Those observations suggest that tannin and bio-oil were crosslinked into a tannin_formaldehyde_bio-oil network compound. The remaining bands on XGL are originated from original biosource materials, tannin or bio-oil.

Table 1. Chemical groups obtained from FTIR analysis of bio-oil and tannin.

Bio-Oil		**Tannin**	
Bonds	Wavenumber (cm^{-1})	Bonds	Wavenumber (cm^{-1})
Aromatic and aliphatic O-H	3800–3000	O-H groups	3800–3000
C-H in methyl and methylene groups	2935, 2845	C-H stretching vibrations	2927
carbonyl in unconjugated C=O	1708		
Phenylpropane skeleton vibrations	1610, 1516, 1462	Aromatic C=C in phenolic groups	1618, 1453
C-O in syringyl groups	1370		
C-H in guayacil rings	1273		
C-H in aromatic rings	1115, 1033	Multisubstituted aromatic rings	1000–750
Aromatic C-H stretching	824	C-H in aromatic rings	841

The essential weight loss of raw materials is most related to the degradation of condensed tannins [41] and lignin [9] compounds. XGL does not present those degradation peaks, showing that those compounds were probably reacted to form the backbone chain of the biopolymer tannin_formaldehyde_bio-oil. In addition, the XGL shows the primary degradation loss (58 wt.%) at 387 °C, which is typical of the decomposition of methylene bridges in phenolic resins [40].

3.2. Evaluation of Costs and Sustainable Characteristics

The gel-like preparation was based on tannin-formaldehyde reactions in a carbon-rich solvent, i.e., the bio-oil. Thus, a sustainable formulation was successfully achieved, as shown in Table 2, producing a 77 wt.% renewable material. The amount of crosslinker (33%), the only synthetic material used to produce the polymeric matrix, is among the lowest employed to prepare gels derived from tannin-formaldehyde systems. Besides, the xerogel-like material produced in this study went through a faster synthesis method than the conventional synthesis of xerogels reported in the literature, usually performed by heating the initial precursor solution for three to seven days.

Table 2. Percentage of renewable materials in the tannin-formaldehyde gel system.

Type of Material	System	Renewable Material (wt%)	Reference
Aerogel	Tannin-formaldehyde	57.5	[24,25]
Xerogel	Tannin-formaldehyde-pluronic	57.5	[23]
Xerogel-like	Tannin-formaldehyde-bio-oil	77.0	This work
Xerogel	Tannin-resorcinol-formaldehyde- sodium dodecyl sulfate	83.2	[21]
Xerogel	Tannin-formaldehyde sodium dodecyl sulfate	89.7	[42]

According to Szczurek et al. [25], the final price of the polymeric resin, i.e., the carbon precursor, is based on the main costs of production following Equation (4):

$$0.8P + 0.04S + 0.19C \quad (4)$$

where P and S are the costs of the precursor and the solvent applied, respectively, and C is the regular costs, such as maintenance, laborers, gases, and energy.

The purified tannin extract (WEIBULL AQ), resorcinol (99%, Sigma Aldrich, 307521-1 KG), and phenol (99%, Sigma Aldrich, 33517-1 KG) cost U$2.70, U$106 and U$232, respectively. Tannin is significantly cheaper than synthetic phenolic precursors. Moreover, no synthetic solvent was employed for either the dissolution of the reactants nor for solvent exchange. Thus, the costs related to the solvent were negligible, and the other costs remained constant. Therefore, the sustainable tannin-bio-oil resin estimated cost is around 5.5 and 5.9 times cheaper than resorcinol-formaldehyde resins and phenol-formaldehyde resins, respectively.

3.3. Textural, Morphological and Structural Properties of XGL-C

The drying method of gels is crucial for producing highly porous materials, and avoiding any shrinkage is still a challenge, especially for materials dried under subcritical conditions; the so-called xerogels. The PMMA microspheres avoided the shrinkage of the polymeric network during the drying process. The volumetric shrinkage values of the sample synthesized with PMMA was 5%, while the sample without PMMA shrank by 42%. The gel-like prepared with PMMA presented a negligible overall shrinkage value comparable to xerogels from tannin-pluronic-formaldehyde (32–90%) [23]. This value is smaller than the smallest values found for aerogels from natural phenolic sources, such as tannin-formaldehyde (30–90%) [24], tannin-lignin-formaldehyde (26–39%) [18], lignin-phenol-formaldehyde (20–70%) [33], soy-flour-tannin-formaldehyde (25–30%) [37], and lignin-oligo (alkylene glycol) (30–60%) [43]. Thus, PMMA behaves as a shrinkage prevention agent, ensuring a lighter and more porous material. The PMMA-based dried

material looks like a hard porous material, while the material with no PMMA had a vitreous aspect. After carbonization and milling, the powder material showed a visual appearance of activated carbon powder. Table 3 presents the textural properties of carbonized (XGL-C) and activated samples (XGL-AC).

Table 3. Chemical composition and textural properties of xerogel-like materials.

Samples	C (%)	H (%)	N (%)	O (%)	S_{BET} (m^2 g^{-1})	$V_{0.97}$ (cm^3 g^{-1})	V_{DR} (cm^3 g^{-1})	V_{meso} (cm^3 g^{-1})	Micro (%)	Meso (%)
XGL-C	84.6	1.1	0.4	13.9	286	0.15	0.11	0.05	69	31
XGL-AC	78.5	1.5	0.2	19.8	808	0.45	0.33	0.15	68	32

The 20 min activation showed an effective increase in the surface area, reaching a value of 808 m^2/g. Figure 2 shows the isotherms of carbonized and activated XGL. The isotherms present type I and IV combinations for both samples [44], exhibiting the typical behavior of micro-mesoporous materials. The desorption branch presented an H4-type hysteresis loop, characteristic of capillary condensation in mesopores [45]. Interestingly, the material showed the same type of isotherm (Figure 2a) and equal proportions of porosity after the activation process, remaining at around 68% and 32% of meso- and microporosity, respectively, indicating a successful activation step.

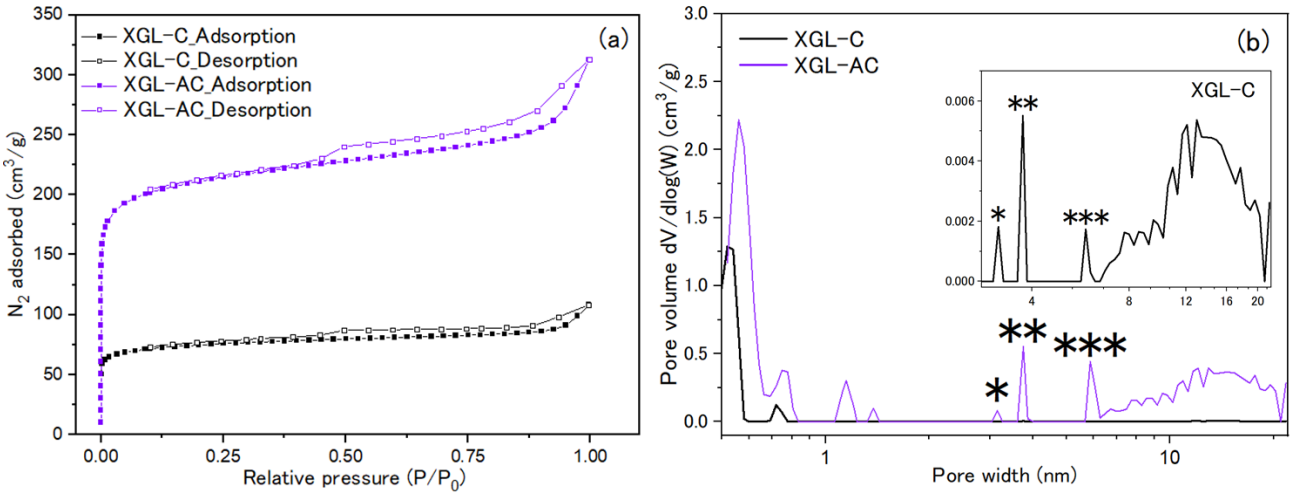

Figure 2. (**a**) Nitrogen adsorption isotherm of XGL-C and XGL-AC and (**b**) pore-size distribution calculated from DFT method. The asterisks are the matching peaks in the inset graph.

Figure 2b shows the corresponding pore size distributions calculated by the DFT model. The carbonized material showed micropores centered at 0.5 and 0.7 nm and mesopores narrower than 20 nm. After activation, the microporosity presented a slight shift to 0.6 and 0.75 nm, respectively. In addition, the activated material presented new pores centered at 1.1 and 1.4 nm and the same mesopores as the carbonized material, but at higher proportions.

Concerning their chemical composition, the carbon materials showed a typical high carbon content, of 78.5% and 84.6%, for XGL-C and XGL-C, respectively. In addition, the percentage of oxygen was relatively higher for the activated material than for the carbonized one (19.8 vs. 13.9%). Both materials also presented a very low amount of hydrogen and nitrogen, respectively, under 2 and 0.5%.

The SEM images in Figure 3 present the microscopic structure of the materials. The photos of XGL-C (Figure 3a,b) and XGL-AC (Figure 3c,d) show a rough surface matrix containing clusters of spherical particles of different sizes. Such agglomerated particles seem to be the typical structures of phenolic gels based on a nodular morphology, generally

arranged in a microscale range and shifted to larger or smaller particles in function of the pH or mass ratio [19]. However, the microscopic structure of xerogel-like materials shown in Figure 3 is composed of nano-nodules particles. In addition, both samples presented an irregular porosity, but the activated material had a more distinct porous structure. These characteristics are observed on the TEM images as well (Figure 3e,f). The porosity is better evaluated on the AC sample, which shows areas with visible parallel channels (red arrows), usually classified as mesopores (pores between 2–50 nm) and found between graphite nanosheets on carbon materials. Furthermore, the activated xerogel-like presents an amorphous structure.

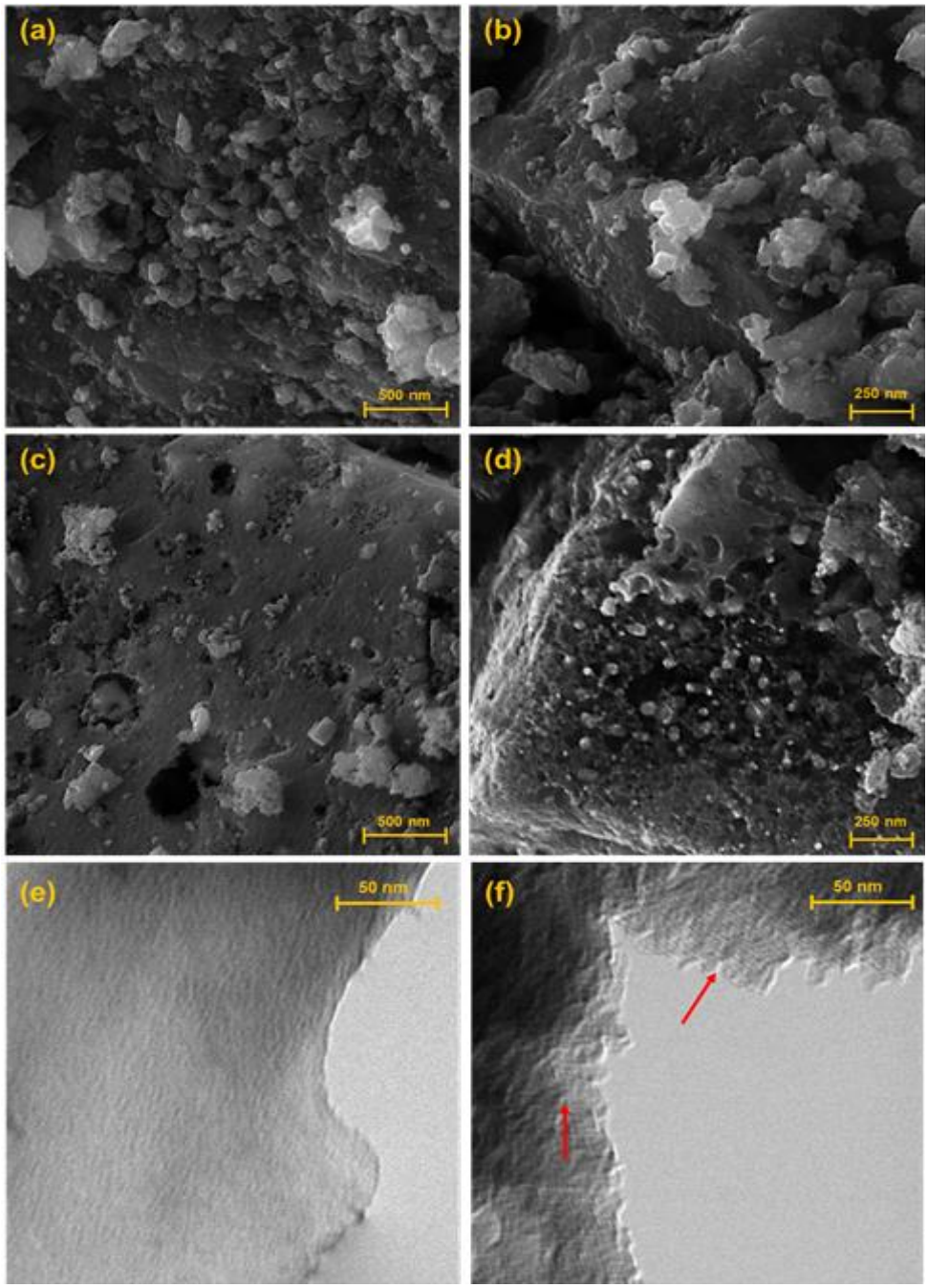

Figure 3. Scanning electron microscopy (SEM) images of XGL-C (**a**,**b**) and XGL-AC (**c**,**d**) and TEM images of XGL-C (**e**) and XGL-AC (**f**).

The structural details from the Raman spectroscopy and the respective deconvolution peaks with five bands for a satisfactory fit are presented in Figure 4a,b, respectively. The first-order parts of the Raman spectra showed two broad bands at 1580 cm^{-1} (G band) and 1320 cm^{-1} (D band), corresponding to the C-C bond vibrations of carbon atoms in an sp2 electronic configuration, and the defect and disorder of structures of carbon materials, respectively [46]. The intensity ratio of the D band to the G band (ID/IG) is a parameter that is often used to estimate the graphitization degree of carbonized materials. Thus, greater graphitization (lower ID/IG) is usually related to higher conductivity and crystallinity materials [47]. As already observed elsewhere [48], this represents the highest disorder structure. Furthermore, the intensity ratio of ID/IG for XGL-C and XGL-AC were 1.12 and 1.24, respectively, measured directly from the envelope of the spectrum and after baseline correction. These findings suggest that the XGL-AC presents a lower graphitic degree, lower conductivity, small ordered structure and higher oxygen functional groups than XGL-C, corroborated by their elemental composition, as observed in Table 3.

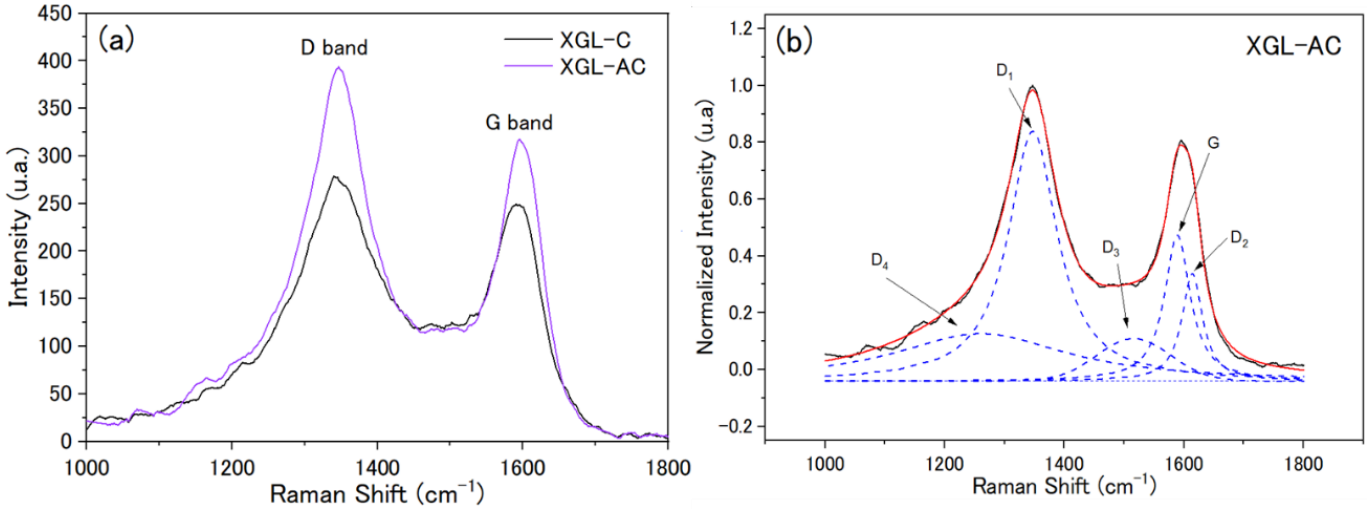

Figure 4. Raman spectra of (**a**) XGL-C and XGL-AC and (**b**) the deconvoluted spectra of XGL-AC.

3.4. Electrochemical Characterizations

The cyclic voltammograms (CV) curves of the XGL-C and XGL-AC electrodes are shown in Figure 5a, in a potential range from −1 to 0 V at a scan rate of 10 mV/s. XGL-AC electrode presents a higher current density amplitude and a rectangular shape, generally attributed to a double-layer contribution. Figure 5b shows the CVs measured at scan rates from 1 mV/s to 100 mV/s. The galvanostatic charge⁄discharge curves (Figure 5c) also indicate that a higher performance storage is achieved by the XGL-AC sample due to the longer discharge time for the same constant current. The electrode specific capacitances (Cs) (Figure 5d) were calculated from the discharge curves using Eq. 1. As expected, XGL-AC presents the highest capacitance values in all current densities applied, reaching a maximum of 132 F/g at 0.1 A/g and an improvement of 43% comparable to the carbonized material XGL-C (92 F/g at 0.1 A/g). This behavior is related to the higher surface area that provides excellent double-layer storage. A low scan rate induces diffusion through the microporous surfaces and, consequently, produces higher capacitance values. In this case, the produced materials might also work as CO_2 capture [49], where low scan rates are required.

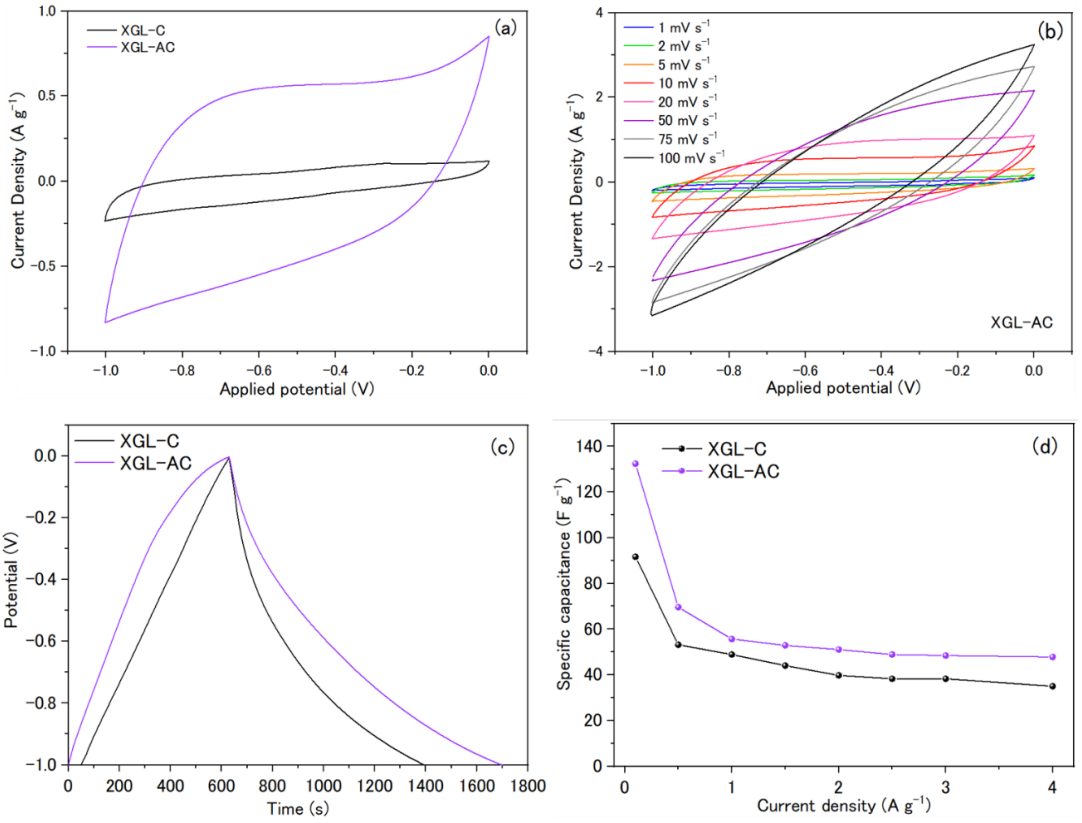

Figure 5. (**a**) CV of carbon electrodes in 6 M KOH electrolyte at 10 mV/s^{-}; (**b**) CV of XGL-AC at scan rates from 1 mV/s to 100 mV/s; (**c**) Charge/discharge galvanostatic curves at current density of 0.1 A/g; (**d**) Specific capacitance of carbon electrodes at different current densities in 6 M KOH.

The electrodes present good long-term cycling stability (Figure 6a) for both samples at a current density of 1 A/g up to 1000 charge/discharge cycles. The stability performances of XGL-C and XGL-AC were quite similar, at 94% and 95%, respectively, showing that no degradation occurs when the current density is constant and indicating their potential use for at least 1000 cycles. The energy density of XGL-C and XGL-AC achieve maximums values of 7.6 Wh/kg and 15.1 Wh/kg at 0.1 Ag, respectively. On the other hand, the maximum power densities at 2.5 A/g were 0.7 kW/kg and 0.4 kW/kg for XGL-C and XGL-AC, respectively. The maximum energy density developed from xerogel-like materials is the second highest compared to other carbons prepared with bio-oil, as observed in Figure 6b.

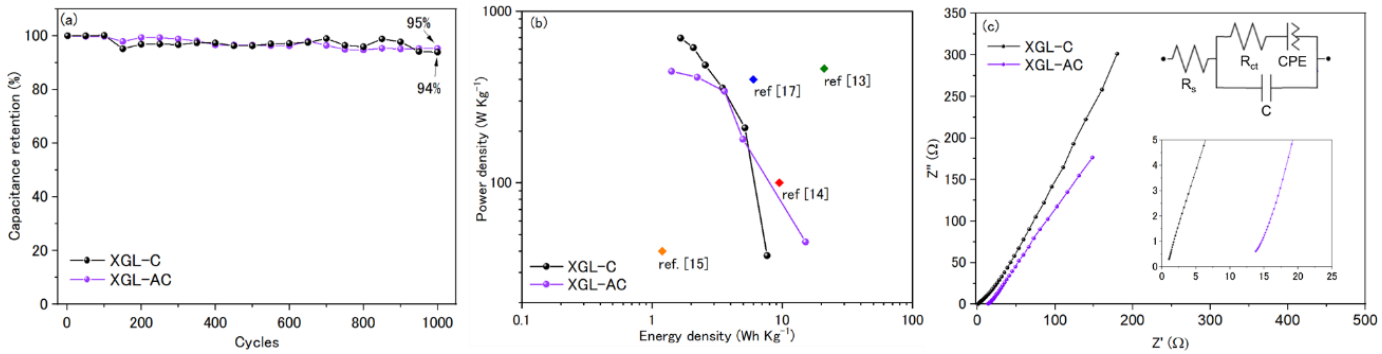

Figure 6. (**a**) Cycling stability of electrodes at 1 A/g and 1 V potential window up to 1000 charge/discharge cycles; (**b**) Energy and power density of the electrodes at current densities ranging from 0.1 to 2.5 A/g; (**c**) Nyquist Plot from EIS.

The electrochemical impedance spectroscopy (EIS) (Figure 6c) presents the Nyquist plots of the electrodes. The high-frequency region (inset graph) usually describes the electrode-electrolyte interface resistance associated with the charge transfer and the double-layer [50]. The total equivalent circuit is described by the equivalent series resistances (Rs), the charge transfer resistance (Rct) and the constant phase angle element (CPE). The XGL-C electrode shows low contact and low equivalent series resistance (1.04 Ω) compared to XGL-AC (13.77 Ω), while the Rct values were very similar, 1.87 Ω to XGL-C and 1.96 Ω to XGL-AC, showing a slightly higher conductivity of the non-activated material. Hence, those specific capacitances of XGL-AC were slightly higher despite the enhanced surface area developed by the physical activation. Furthermore, both samples presented the 45° slope at a low frequency related to the resistance diffusion of ions on the interface/interior of the tiny pores, typical of porous carbon electrodes [51].

As seen in Table 4, the produced xerogel-like materials from bio-oil present capacitance values that still need improvement. However, the other materials exhibiting higher capacitance values present several steps for preparation, such as chemical activation, N-doping by using ammonia gas or melamine, and synthetic chemicals as template agents. Thus, the use of templates and the activation process with KOH require washing steps to prepare the material. This washing uses corrosive solutions of HCL to remove the templates and the impurities after activation reactions. In addition, it is followed by pure water washing, thus increasing the final cost of the product. Therefore, the xerogel-like materials presented in this study stand out as a simple, cheap production route with a high renewable feature, meeting the current environmental requirements laws.

Table 4. Synthesis steps, electrochemical performance and S_{BET} of carbons prepared with bio-oil from different bio-sources.

Bio-Oil Source	Carbon Material	Additional Chemicals	Chemical Activator	Electrolyte	C_S (F/g)	Current Density (A/g)	S_{BET} (m^2/g)	References
Grapeseed	Nitrogen-doped carbon nano-onion	Gas NH_3 (Ns)	KOH	2 M KOH	54 *	0.1	116	[15]
Pine granule	Bio-oil derived hierarchical porous carbon	Nano-MgO (p-a.a)	-	6 M KOH	344 **	0.5	1409	[17]
Poplar wood sawdust	Bio-oil honeycomb carbon	Cetyltrimethy-lammonium bromide (p-a.a)	KOH	6 M KOH	312 **	1	1302	[14]
Poplar wood sawdust	Nitrogen-doped porous carbon nanosheet	Melamine (Ns)	KOH	6 M KOH	289 **	0.5	2566	[13]
Tilia Americana wood waste	Xerogel-like carbon	-	-	6 M KOH	92 **	0.1	286	This work
Tilia Americana wood waste	Xerogel-like activated carbon	-	CO_2	6 M KOH	132 **	0.1	808	This work

Ns = nitrogen source; p-a.a = pore-adjusting agent; * single T-type cell; ** three- electrode system.

4. Conclusions

This paper demonstrated a simple gel-like preparation based on tannin-formaldehyde reactions. The production process took few hours to generate a gel-like material with an enhanced sustainable feature. Tannin-formaldehyde reactions were preferred to obtain a cheap, renewable porous material, replacing the synthetic phenolic systems based on costly and toxic precursors such as resorcinol or phenol. Furthermore, the use of a carbon-rich by-product like bio-oil as a solvent to this system reaction, and the PMMA as a shrinkage prevention agent, were reported for the first time, resulting in an innovative process to produce a cheap, highly renewable porous carbon. The proposed methodology resulted in materials with a high sustainable fraction (77 wt.%) and a significant low-cost value compared to synthetic resins, promoting large-scale advances.

Activating the material for 20 min enhanced the effective electrochemical material by about 43% (132 F/g vs. 92 F/g) but presented a resistive behavior compared to the non-activated material. The activated material also provided good performances in electrochemical analysis by achieving a significant energy density value of 15.1 Wh/kg, comparable to other bio-oil carbons. Further work should be carried out to: (i) optimize the synthesis parameters (e.g., different pHs, activation conditions) to improve gels surface area; (ii) replace formaldehyde with a crosslinking agent that is less toxic to consequently reach a 100% renewable material; and (iii) test the xerogel-like materials with high microporosity surface as CO_2 capture and contaminant sorption in drinking water and wastewater.

Author Contributions: Conceptualization, G.A.-L. and F.L.B.; methodology, G.A.-L.; investigation, G.A.-L., M.G.C.M., B.C.d.S.F. and P.d.A.-M.; resources, G.F.B.L.e.S. and M.R.B.; data curation, G.A.-L. and M.G.C.M.; writing—original draft preparation, A.F.N.B.; writing—review and editing, G.A.-L., A.F.N.B. and F.L.B.; visualization, G.A.-L., and A.F.N.B.; supervision, A.K., H.B., G.F.B.L.e.S. and M.R.B.; project administration, G.A.-L.; funding acquisition, A.K., H.B., G.F.B.L.e.S. and M.R.B. All authors have read and agreed to the published version of the manuscript.

Funding: This research received no external funding.

Institutional Review Board Statement: Not applicable.

Informed Consent Statement: Not applicable.

Data Availability Statement: The data presented in this study are available on request from the corresponding author. Also, the data are not publicly available because they are being processed for other publications.

Acknowledgments: G.A.-L. acknowledges financial support by CNPq. A.F.N.B. (grant n° 88887.358274/2019-00) and P.d.A.-M. (grant n° 88882.315554/2019-01) thank PNPD/CAPES for the financial support. M.G.C.M (grant n° 88887.631486/2021-00) and B.C.d.S.F. (grant n° 88882.444518/2019-01) thank the Coordenação de Aperfeiçoamento de Pessoal de Nível Superior (CAPES)-Brazil.

Conflicts of Interest: The authors declare no conflict of interest.

References

1. Hall, P.J.; Bain, E.J. Energy-storage technologies and electricity generation. *Energy Policy* **2008**, *36*, 4352–4355. [CrossRef]
2. Yin, J.; Zhang, W.; Alhebshi, N.A.; Salah, N.; Alshareef, H.N. Synthesis Strategies of Porous Carbon for Supercapacitor Applications. *Small Methods* **2020**, *4*, 1900853. [CrossRef]
3. Liu, B.; Shioyama, H.; Akita, T.; Xu, Q. Metal-Organic Framework as a Template for Porous Carbon Synthesis. *J. Am. Chem. Soc.* **2008**, *130*, 5390–5391. [CrossRef]
4. Pachfule, P.; Shinde, D.; Majumder, M.; Xu, Q. Fabrication of carbon nanorods and graphene nanoribbons from a metal–organic framework. *Nat. Chem.* **2016**, *8*, 718–724. [CrossRef]
5. Weber, K.; Quicker, P. Properties of biochar. *Fuel* **2018**, *217*, 240–261. [CrossRef]
6. Singh, G.; Lakhi, K.S.; Sil, S.; Bhosale, S.V.; Kim, I.; Albahily, K.; Vinu, A. Biomass derived porous carbon for CO2 capture. *Carbon* **2019**, *148*, 164–186. [CrossRef]
7. Joseph, S.D.; Camps-Arbestain, M.; Lin, Y.; Munroe, P.; Chia, C.H.; Hook, J.; van Zwieten, L.; Kimber, S.; Cowie, A.; Singh, B.P.; et al. An investigation into the reactions of biochar in soil. *Soil Res.* **2010**, *48*, 501. [CrossRef]
8. Inyang, M.I.; Gao, B.; Yao, Y.; Xue, Y.; Zimmerman, A.; Mosa, A.; Pullammanappallil, P.; Ok, Y.S.; Cao, X. A review of biochar as a low-cost adsorbent for aqueous heavy metal removal. *Crit. Rev. Environ. Sci. Technol.* **2016**, *46*, 406–433. [CrossRef]

9. Saffar, T.; Bouafif, H.; Braghiroli, F.L.; Magdouli, S.; Langlois, A.; Koubaa, A. Production of Bio-based Polyol from Oxypropylated Pyrolytic Lignin for Rigid Polyurethane Foam Application. *Waste Biomass Valorization* **2020**, *11*, 6411–6427. [CrossRef]
10. Pinheiro Pires, A.P.; Arauzo, J.; Fonts, I.; Domine, M.E.; Fernández Arroyo, A.; Garcia-Perez, M.E.; Montoya, J.; Chejne, F.; Pfromm, P.; Garcia-Perez, M. Challenges and Opportunities for Bio-oil Refining: A Review. *Energy Fuels* **2019**, *33*, 4683–4720. [CrossRef]
11. Xiu, S.; Shahbazi, A. Bio-oil production and upgrading research: A review. *Renew. Sustain. Energy Rev.* **2012**, *16*, 4406–4414. [CrossRef]
12. Sanchez-Sanchez, A.; Izquierdo, M.T.; Mathieu, S.; Medjahdi, G.; Fierro, V.; Celzard, A. Activated carbon xerogels derived from phenolic oil: Basic catalysis synthesis and electrochemical performances. *Fuel Process. Technol.* **2020**, *205*, 106427. [CrossRef]
13. Wang, Q.; Qin, B.; Zhang, X.; Xie, X.; Jin, L.; Cao, Q. Synthesis of N-doped carbon nanosheets with controllable porosity derived from bio-oil for high-performance supercapacitors. *J. Mater. Chem. A* **2018**, *6*, 19653–19663. [CrossRef]
14. Wang, Q.; Qin, B.; Li, H.-X.; Zhang, X.-H.; Tian, X.; Jin, L.; Cao, Q. Honeycomb-like carbon with tunable pore size from bio-oil for supercapacitor. *Microporous Mesoporous Mater.* **2020**, *309*, 110551. [CrossRef]
15. Shaku, B.; Mofokeng, T.P.; Mongwe, T.H.; Coville, N.J.; Ozoemena, K.I.; Maubane-Nkadimeng, M.S. Physicochemical Properties of Nitrogen Doped Carbon Nano-onions Grown by Flame Pyrolysis from Grapeseed Oil for Use in Supercapacitors. *Electroanalysis* **2020**, *32*, 2946–2957. [CrossRef]
16. Fan, H.; Zhou, S.; Li, Q.; Gao, G.; Wang, Y.; He, F.; Hu, G.; Hu, X. Hydrogen-bonded frameworks crystals-assisted synthesis of flower-like carbon materials with penetrable meso/macropores from heavy fraction of bio-oil for Zn-ion hybrid supercapacitors. *J. Colloid Interface Sci.* **2021**, *600*, 681–690. [CrossRef]
17. Li, J.; Xiao, R.; Li, M.; Zhang, H.; Wu, S.; Xia, C. Template-synthesized hierarchical porous carbons from bio-oil with high performance for supercapacitor electrodes. *Fuel Process. Technol.* **2019**, *192*, 239–249. [CrossRef]
18. Grishechko, L.I.; Amaral-Labat, G.; Szczurek, A.; Fierro, V.; Kuznetsov, B.N.; Pizzi, A.; Celzard, A. New tannin-lignin aerogels. *Ind. Crops Prod.* **2013**, *41*. [CrossRef]
19. Braghiroli; Amaral-Labat; Boss; Lacoste; Pizzi Tannin Gels and Their Carbon Derivatives: A Review. *Biomolecules* **2019**, *9*, 587. [CrossRef]
20. Pizzi, A. Tannins: Prospectives and Actual Industrial Applications. *Biomolecules* **2019**, *9*, 344. [CrossRef]
21. Rey-Raap, N.; Szczurek, A.; Fierro, V.; Menéndez, J.A.; Arenillas, A.; Celzard, A. Towards a feasible and scalable production of bio-xerogels. *J. Colloid Interface Sci.* **2015**, *456*, 138–144. [CrossRef]
22. Amaral-Labat, G.; Szczurek, A.; Fierro, V.; Celzard, A. Unique bimodal carbon xerogels from soft templating of tannin. *Mater. Chem. Phys.* **2015**, *149–150*, 193–201. [CrossRef]
23. Amaral-Labat, G.; Grishechko, L.I.; Fierro, V.; Kuznetsov, B.N.; Pizzi, A.; Celzard, A. Tannin-based xerogels with distinctive porous structures. *Biomass Bioenergy* **2013**, *56*, 437–445. [CrossRef]
24. Amaral-Labat, G.; Szczurek, A.; Fierro, V.; Pizzi, A.; Celzard, A. Systematic studies of tannin–formaldehyde aerogels: Preparation and properties. *Sci. Technol. Adv. Mater.* **2013**, *14*, 015001. [CrossRef] [PubMed]
25. Szczurek, A.; Amaral-Labat, G.; Fierro, V.; Pizzi, A.; Masson, E.; Celzard, A. The use of tannin to prepare carbon gels. Part I: Carbon aerogels. *Carbon N. Y.* **2011**, *49*, 2773–2784. [CrossRef]
26. Brunauer, S.; Emmett, P.H.; Teller, E. Adsorption of Gases in Multimolecular Layers. *J. Am. Chem. Soc.* **1938**, *60*, 309–319. [CrossRef]
27. Dubinin, M.M. Fundamentals of the theory of adsorption in micropores of carbon adsorbents: Characteristics of their adsorption properties and microporous structures. *Carbon* **1989**, *27*, 457–467. [CrossRef]
28. Yun, M.H.; Yeon, J.W.; Hwang, J.; Hong, C.S.; Song, K. A calibration technique for an Ag/AgCl reference electrode utilizing the relationship between the electrical conductivity and the KCl concentration of the internal electrolyte. *J. Appl. Electrochem.* **2009**, *39*, 2587–2592. [CrossRef]
29. Abdul-Aziz, M.R.R.; Hassan, A.; Abdel-Aty, A.A.R.; Saber, M.R.; Ghannam, R.; Anis, B.; Heidari, H.; Khalil, A.S.G. High Performance Supercapacitor Based on Laser Induced Graphene for Wearable Devices. *IEEE Access* **2020**, *8*, 200573–200580. [CrossRef]
30. Scholze, B.; Meier, D. Characterization of the water-insoluble fraction from pyrolysis oil (pyrolytic lignin). Part I. PY–GC/MS, FTIR, and functional groups. *J. Anal. Appl. Pyrolysis* **2001**, *60*, 41–54. [CrossRef]
31. Turunen, M.; Alvila, L.; Pakkanen, T.T.; Rainio, J. Modification of phenol-formaldehyde resol resins by lignin, starch, and urea. *J. Appl. Polym. Sci.* **2003**, *88*, 582–588. [CrossRef]
32. Sarathchandran, C.; Ilangovan, S.A. Carbon aerogels: Synthesis, properties, and applications. In *Handbook of Carbon-Based Nanomaterials*; Elsevier: Amsterdam, The Netherlands, 2021; pp. 739–781.
33. Grishechko, L.I.; Amaral-Labat, G.; Szczurek, A.; Fierro, V.; Kuznetsov, B.N.; Celzard, A. Lignin-phenol-formaldehyde aerogels and cryogels. *Microporous Mesoporous Mater.* **2013**, *168*, 19–29. [CrossRef]
34. Lu, Q.; Zhang, J.; Zhu, X. Corrosion properties of bio-oil and its emulsions with diesel. *Chinese Sci. Bull.* **2008**, *53*, 3726–3734. [CrossRef]
35. Szczurek, A.; Amaral-Labat, G.; Fierro, V.; Pizzi, A.; Celzard, A. The use of tannin to prepare carbon gels. Part II. Carbon cryogels. *Carbon* **2011**, *49*, 2785–2794. [CrossRef]

36. Amaral-Labat, G.; da Silva, E.L.; Cuña, A.; Malfatti, C.F.; Marcuzzo, J.S.; Baldan, M.R.; Celzard, A.; Fierro, V.; Lenz e Silva, G.F.B. A Sustainable Carbon Material from Kraft Black Liquor as Nickel-Based Electrocatalyst Support for Ethanol Electro-Oxidation. *Waste Biomass Valorization* **2020**, *12*, 2507–2519. [CrossRef]
37. Amaral-Labat, G.; Grishechko, L.; Szczurek, A.; Fierro, V.; Pizzi, A.; Kuznetsov, B.; Celzard, A. Highly mesoporous organic aerogels derived from soy and tannin. *Green Chem.* **2012**, *14*, 3099–3106. [CrossRef]
38. Paysepar, H.; Hu, Y.; Feng, S.; Yuan, Z.; Shui, H.; Xu, C. (Charles) Bio-phenol formaldehyde (BPF) resoles prepared using phenolic extracts from the biocrude oils derived from hydrothermal liquefaction of hydrolysis lignin. *React. Funct. Polym.* **2020**, *146*, 104442. [CrossRef]
39. Li, B.; Yuan, Z.; Schmidt, J.; Xu, C.C. New foaming formulations for production of bio-phenol formaldehyde foams using raw kraft lignin. *Eur. Polym. J.* **2019**, *111*, 1–10. [CrossRef]
40. Celikbag, Y.; Nuruddin, M.; Biswas, M.; Asafu-Adjaye, O.; Via, B.K. Bio-oil-based phenol–formaldehyde resin: Comparison of weight- and molar-based substitution of phenol with bio-oil. *J. Adhes. Sci. Technol.* **2020**, *34*, 2743–2754. [CrossRef]
41. Sebestyén, Z.; Jakab, E.; Badea, E.; Barta-Rajnai, E.; Şendrea, C.; Czégény, Z. Thermal degradation study of vegetable tannins and vegetable tanned leathers. *J. Anal. Appl. Pyrolysis* **2019**, *138*, 178–187. [CrossRef]
42. Rey-Raap, N.; Szczurek, A.; Fierro, V.; Celzard, A.; Menéndez, J.A.; Arenillas, A. Advances in tailoring the porosity of tannin-based carbon xerogels. *Ind. Crops Prod.* **2016**, *82*, 100–106. [CrossRef]
43. Perez-Cantu, L.; Liebner, F.; Smirnova, I. Preparation of aerogels from wheat straw lignin by cross-linking with oligo(alkylene glycol)-α,ω-diglycidyl ethers. *Microporous Mesoporous Mater.* **2014**, *195*, 303–310. [CrossRef]
44. Celzard, A.; Fierro, V.; Amaral-Labat, G. Adsorption by Carbon Gels. In *Novel Carbon Adsorbents*; Elsevier: Amsterdam, The Netherlands, 2012; ISBN 9780080977447.
45. Thommes, M.; Kaneko, K.; Neimark, A.V.; Olivier, J.P.; Rodriguez-Reinoso, F.; Rouquerol, J.; Sing, K.S.W. Physisorption of gases, with special reference to the evaluation of surface area and pore size distribution (IUPAC Technical Report). *Pure Appl. Chem.* **2015**, *87*, 1051–1069. [CrossRef]
46. Shimodaira, N.; Masui, A. Raman spectroscopic investigations of activated carbon materials. *J. Appl. Phys.* **2002**, *92*, 902–909. [CrossRef]
47. Elaiyappillai, E.; Srinivasan, R.; Johnbosco, Y.; Devakumar, P.; Murugesan, K.; Kesavan, K.; Johnson, P.M. Low cost activated carbon derived from Cucumis melo fruit peel for electrochemical supercapacitor application. *Appl. Surf. Sci.* **2019**, *486*, 527–538. [CrossRef]
48. Bratek, W.; Świątkowski, A.; Pakuła, M.; Biniak, S.; Bystrzejewski, M.; Szmigielski, R. Characteristics of activated carbon prepared from waste PET by carbon dioxide activation. *J. Anal. Appl. Pyrolysis* **2013**, *100*, 192–198. [CrossRef]
49. Hao, G.-P.; Li, W.-C.; Lu, A.-H. Novel porous solids for carbon dioxide capture. *J. Mater. Chem.* **2011**, *21*, 6447–6451. [CrossRef]
50. Bhattacharjya, D.; Yu, J.-S. Activated carbon made from cow dung as electrode material for electrochemical double layer capacitor. *J. Power Sources* **2014**, *262*, 224–231. [CrossRef]
51. Chang, B.; Guo, Y.; Li, Y.; Yin, H.; Zhang, S.; Yang, B.; Dong, X. Graphitized hierarchical porous carbon nanospheres: Simultaneous activation/graphitization and superior supercapacitance performance. *J. Mater. Chem. A* **2015**, *3*, 9565–9577. [CrossRef]